Kinetic Characterization of Wild-Type and S229A Mutant MurB: Evidence for the Role of Ser 229 as a General Acid†

Timothy E. Benson,‡ Christopher T. Walsh,*,‡ and Vincent Massey§

Department of Biological Chemistry and Molecular Pharmacology, Harvard Medical School, 240 Longwood Avenue, Boston, Massachusetts 02115, and Department of Biological Chemistry, The University of Michigan Medical School, 1301 Catherine Road, Ann Arbor, Michigan 48109

Received August 30, 1996⊗

ABSTRACT: X-ray derived structural data predicted that serine 229 was positioned to act as a proton donor to the developing C2 carbanion during the reduction of enolpyruvyl-UDP-*N*-acetylglucosamine catalyzed by the bacterial peptidoglycan biosynthetic flavoenzyme MurB. To investigate this effect, a mutant where serine 229 was replaced by alanine was constructed and purified. Kinetic analysis of the two half-reactions for the mutant enzyme revealed a 9-fold decrease in the reduction of EFl_{ox} by NADPH and a dramatic 10^7-fold decrease in the reoxidation of EFl_{red} with the enolpyruvyl substrate. In addition, studies of S229A with the substrate analog, *(E)*-enolbutyryl-UDP-*N*-acetylglucosamine, showed a striking bias of the partitioning toward formation of the *(Z)* geometric isomer as opposed to formation of the reduced product UDP-methylmuramic acid, which was the predominant product in wild-type MurB. These studies provide evidence for the proposed role of this active-site serine as a general acid catalyst.

Both Gram-positive and Gram-negative bacteria possess a unique biopolymer, peptidoglycan, critical for maintaining the osmotic integrity of the cell. The peptidoglycan is comprised of tandem repeats of two sugars, *N*-acetylglucosamine and *N*-acetylmuramic acid, and a four- or five-residue peptide chain containing a lysine or diaminopimelate residue which enables interpeptide cross-linking (Park, 1987). The synthesis of the UDP precursor of *N*-acetylmuramic acid is a central part of peptidoglycan biosynthesis since the lactyl ether stem (circled in Figure 1) of the muramic acid portion of the disaccharide serves as the connector of the sugar and peptide portions of the peptidoglycan.

UDP-*N*-acetylmuramic acid is synthesized *in vivo* by the sequential action of MurA, UDP-*N*-acetylglucosaminenolpyruvyl transferase, which catalyzes an enolpyruvyl transfer from phosphoenolpyruvate to the 3′-hydroxyl of UDP-*N*-acetylglucosamine, and MurB, UDP-*N*-acetylenolpyruvylglucosamine reductase, which reduces the enolpyruvyl moiety to the lactyl ether of UDP-*N*-acetylmuramic acid (Bugg & Walsh, 1993). We have shown previously that MurB is a flavoprotein which utilizes its bound flavin adenine dinucleotide (FAD)[1] cofactor as a mediator for two-electron transfer from NADPH to the FAD in the first half-reaction. In the second half-reaction the same two electrons are transferred from the $FADH_2$ to the C3 of the enol ether and the reduction of the vinyl bond is completed by quenching at C2 of the carbanion equivalent with a solvent-exchangeable proton (Benson et al., 1993) (Figure 2). Based on precedents from mechanistic work on mandelate racemase and other enzymes which abstract a proton α to a carboxylate (the reverse reaction of the second step of MurB's reduction of the enol ether) (Gerlt & Gassman, 1992, 1993) and X-ray crystallographic analysis of the MurB−EP-UDP-GlcNAc complex, we have proposed stabilization of the carbanion intermediate as an enol by hydrogen-bonding to Glu 325 and/or Arg 159 (Benson et al., 1995). The existence of this carbanion as a long-lived intermediate and the stepwise reduction of the vinyl bond by hydride transfer and protonation was recently proposed on the basis of isomerization activity of MurB in forming *(Z)*-EB-UDP-GlcNAc from *(E)*-EB-UDP-GlcNAc (Lees et al., 1996). In those experiments, D_2O was found to increase the proportion of partitioning to the isomerized substrate, *(Z)*-EB-UDP-GlcNAc, and away from the reduced product, UDP-Me-MurNAc, by a factor of 1.8. This result indicated that the presence of D_2O affected the protonation step in the reduction of the *(E)*-EB-UDP-GlcNAc substrate.

The X-ray crystal structure of the MurB-EP-UDP-GlcNAc complex clearly shows Ser 229 at a distance of 3.1 Å from C2 in a prime orientation to serve as the proton donor to quench the carbanion/enol intermediate and deliver the proton at C2 to yield the D-configuration of the lactyl ether product. The proposed role of Ser 229 as a proton donor is unusual because the pK_a of serine is between 13 and 15, making donation of a proton during catalysis at neutral pH energetically unfavorable. However, there is precedent for removal of the serine hydroxyl proton to form an alkoxide anion

† This work was supported in part by National Institutes of Health Grant GM49338 (C.T.W.) and GM11106 (V.M.).

‡ Harvard Medical School.

§ University of Michigan Medical School.

⊗ Abstract published in *Advance ACS Abstracts,* January 15, 1997.

[1] Abbreviations: (*E*)-EB-UDP-GlcNAc, uridine 5′-(trihydrogen diphosphate), *P*′-[2-(acetylamino)-3-*O*-[(*E*)-1-carboxyprop-1-enyl]-2-deoxy-α-D-glucopyranosyl] ester; (*Z*)-EB-UDP-GlcNAc, uridine 5′-(trihydrogen diphosphate), *P*′-[2-(acetylamino)-3-*O*-((*Z*)-1-carboxyprop-1-enyl]-2-deoxy-α-D-glucopyranosyl] ester; FAD, flavin adenine dinucleotide; EP-UDP-GlcNAc, uridine 5′-(trihydrogen diphosphate), *P*′-[2-(acetylamino)-3-*O*-[(*E*)-1-carboxyeth-1-enyl]-2-deoxy-α-D-glucopyranosyl] ester; HEPES, (4-[2-hydroxyethyl]-1-piperazineethanesulfonic acid); $NADP^+$, oxidized β-nicotinamide adenine dinucleotide phosphate; NADPH, reduced β-nicotinamide adenine dinucleotide phosphate; NMR, nuclear magnetic resonance; PEP, phosphoenolpyruvate; UDP-Me-MurNAc, uridine 5′-(trihydrogen diphosphate), *P*′-[2-(acetylamino)-3-*O*-(1-*R*-carboxypropyl)-2-deoxy-α-D-glucopyranosyl] ester; UDP-MurNAc, uridine 5′-(trihydrogen diphosphate), *P*′-[2-(acetylamino)-3-*O*-(1-*R*-carboxyethyl)-2-deoxy-α-D-glucopyranosyl] ester.

S0006-2960(96)02220-9 CCC: $14.00

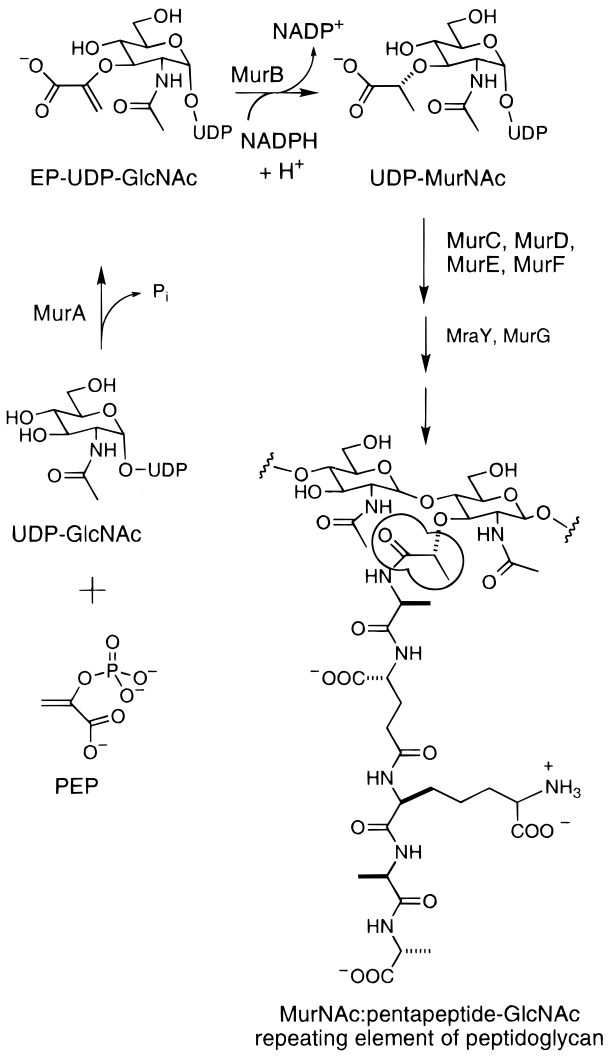

FIGURE 1: First two steps in peptidoglycan biosynthesis, showing the formation of the lactyl ether stem (circled) which bridges between the disaccharide and peptide portions of peptidoglycan.

equivalent in serine proteases and kinases. In these cases, the serine alkoxide is generated as a transition state by concerted acid−base catalysis in order that the alkoxide equivalent may act as a nucleophile. In the case of the serine proteases, an adjacent histidine and aspartic acid stabilize the transition state involving the serine anion (Walsh, 1979). The role proposed for serine in MurB is somewhat different as it requires serine to act as an electrophile (Figure 3). This role is analogous to the proposed alkoxide ion transition state, yet instead the anion equivalent reacts not as a nucleophile toward a carbon or phosphorus atom but as an acid−base in proton transfer.

To investigate the role of Ser 229, a serine to alanine mutant (S229A) was constructed. If Ser 229 serves as a proton transfer catalyst as in Figure 3, one would expect S229A to be competent for reduction of the enzyme-bound FAD by NADPH, but either substantially less or completely incompetent in the oxidative half-reaction with either the EP-UDP-GlcNAc or *(E)*-EB-UDP-GlcNAc substrates. The solvent isotope product-determining effect observed during catalysis with the substrate *(E)*-EB-UDP-GlcNAc (Lees et al., 1996) should also be affected in a S229A mutant in favor of isomerization. Kinetic and NMR studies described here with both EP-UDP-GlcNAc and *(E)*-EB-UDP-GlcNAc explore the specific effects the alanine mutant has on catalysis and provide evidence for the proposed role of Ser 229 as a general acid catalyst.

EXPERIMENTAL PROCEDURES (MATERIALS AND METHODS)

Wild-type MurB was purified as described previously (Benson et al., 1993, 1994). NADPH and $NADP^+$ were obtained from Sigma Chemical Co. (St. Louis, MO). Spectroscopy was carried out either with a Hewlett-Packard diode array spectrophotometer (Model 8452A) or with a Perkin Elmer Lamba 6 spectrophotometer. Synthesis of *(E)*-EB-UDP-GlcNAc was carried out as described previously (Lees & Walsh, 1995).

PCR Mutagenesis for S229A. Two sets of primers were synthesized (Integrated DNA Technologies, Inc, Coralville, IA). The first set included a primer (5′-CGGAATTCCTG-CAGAAGGAGATATACA-3′) corresponding to the sequence 5′ to the *murB* gene containing an *Eco*RI site (underlined) from the polylinker as it was previously cloned into the pKEN vector [pTEB004 (Benson et al., 1993)] and a second primer (5′-CAACAGGGTTTTTGAAGAAA**GC**ACCGGCATTGCCATTCACTT-3′) complementary to the opposite strand in the region where the S229A mutation was to be introduced. This second primer contained the AG → GC base changes (in boldface type) in order to introduce two mutations at bases 685 and 686 of the *murB* gene. The second set of primers included a 5′ primer (5′-AAGTGAAT GGCAATGCCGGT**GC**TTTCTTCAAAAACCCTGTTG-3′), which was complementary to the first mutant primer, and a second primer (5′-GCTCTAGAAATTTCAGTG-GCACGGTGT-3′) corresponding to the 3′ end of the *murB* gene including the *Xba*I site (underlined) from the polylinker region.

For all PCR reactions Vent DNA polymerase (New England Biolabs) was used. In the first round of PCR (15 cycles), each pair of primers was used in separate reactions to amplify two halves of the mutated *murB* gene which contained a 20-bp overlap with each other. The PCR products were purified on a 1.5% agarose gel and extracted from the argarose using a Qiaex II gel extraction kit (Qiagen). In a second round of PCR (15 cycles), the reaction included the two products from the first round of PCR along with the *Eco*RI and *Xba*I primers corresponding to the 5′ and 3′ ends of the *murB* gene. This second PCR product was purified as in round one. The purified 1-kb fragment was digested with *Eco*RI and *Xba*I and ligated for 3 h at 16 °C into pKEN vector which had been cut with the same enzymes. The ligation reaction was transformed into XA90 cells. DNA sequencing of the 1-kb insert to confirm the incorporation of the two mutations at bases 685−686 and lack of PCR mutations was performed with an Applied Biosystems Model 373A automated DNA sequencer using dye-labeled dideoxy nucleotides (Biopolymers Facilities, Howard Hughes Medical Institute, Harvard Medical School).

Redox Potential. The redox potentials for the wild-type enzyme and S229A mutant were measured as described (Massey, 1990). Briefly, enzyme was diluted into 100 mM potassium phosphate buffer, pH 7.0, along with 12 μM phenosafranin, 150 μM xanthine, and 10 μM methyl viologen at 25 °C. After the mixture was made anaerobic by at least 10 rounds of evacuation and purging with argon, a solution of xanthine oxidase was added. Spectra were taken at least

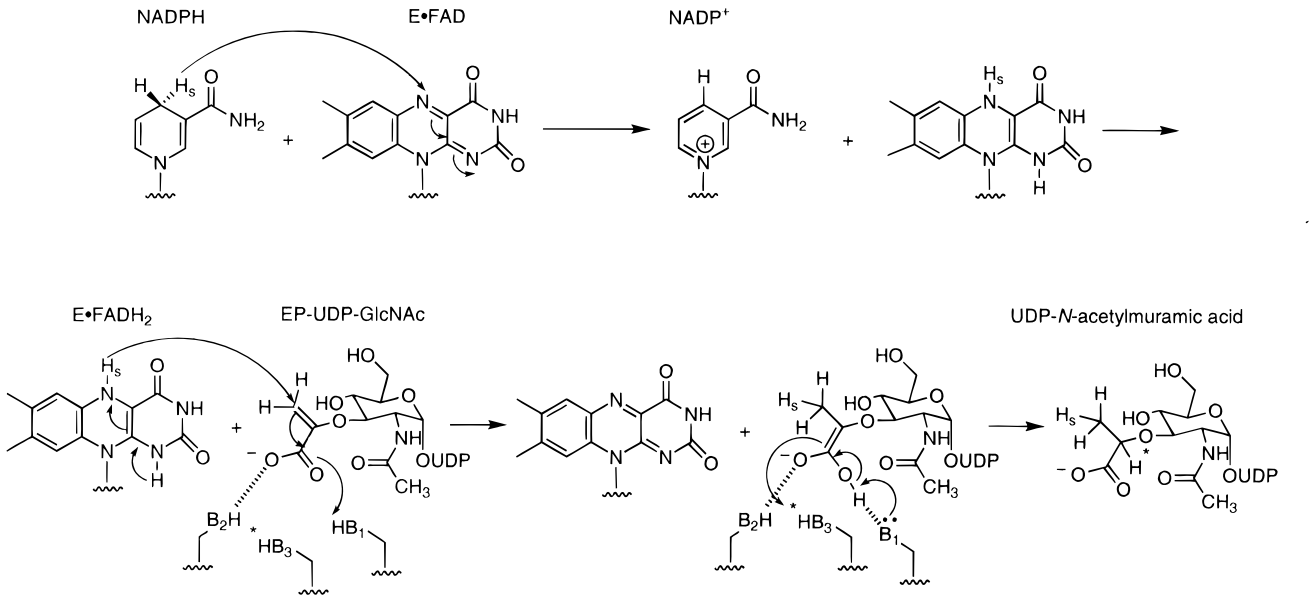

FIGURE 2: Reductive and oxidative half-reactions of MurB.

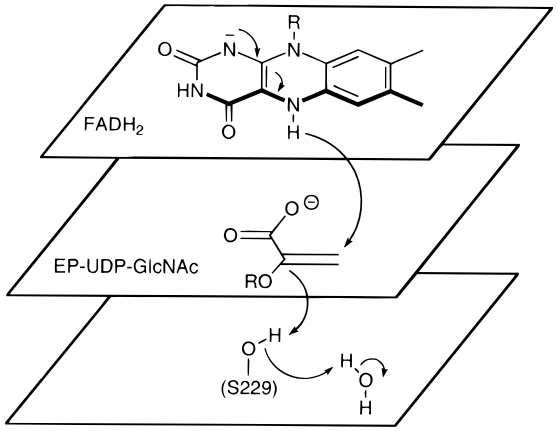

FIGURE 3: Proposed mechanistic role for Ser 229 as a proton transfer catalyst to C2 of EP-UDP-GlcNAc.

every 4 min until reduction of MurB was complete. The reduction potential was calculated by plotting the logarithm of the ratio of oxidized to reduced phenosafranin versus the logarithm of the ratio of oxidized to reduced MurB. The point at which there was an equimolar amount of oxidized and reduced forms of MurB present in the mixture (log ox/red is zero) gives the ΔE_m of MurB from the known phenosafranin (redox potential of −252 mV).

Stopped-Flow Absorbance Spectroscopy. All experiments were conducted at 25 °C in 50 mM Tris-HCl, pH 8.0, and 20 mM KCl. Stopped-flow experiments were conducted using a Hi-Tech (U.K.) syringe apparatus and a Jarrell-Ash monochromator interfaced with a computer, as has been described previously (Beaty & Ballou, 1981). Oxygen was eliminated from the stopped-flow apparatus by treating the syringes overnight with an anaerobic solution of 3,4-dihydroxybenzoate and protocatechuate-3,4-dioxygenase (a generous gift of Dr. David P. Ballou, University of Michigan). Buffer and substrate solutions were made anaerobic by sparging argon through the solution for at least 15 min before introduction to the stopped-flow apparatus. Wild-type and mutant enzyme were made anaerobic in a tonometer with alternating rounds of evacuation and purging with argon. Fluorescence stopped-flow experiments were conducted with a Kinetics Instruments apparatus as described previously (Brissette et al., 1989). This instrument has a dead time of approximately 1 ms.

Data collection and determination of rate constants were conducted by the software package Program A developed by C.-J. Chiu, R. Chung, J. Dinverno, and D. P. Ballou, University of Michigan. Program A carries out fitting of experimental data to exponential rate equations using the Marquardt algorithm (Bevington, 1969) where up to five rate constants can be fixed.

Anaerobic Reduction of MurB. In order to study the oxidative half-reaction, wild-type MurB was reduced slightly less than stoichiometrically in an anaerobic tonometer by titration with a 10 mM solution of dithionite. Substoichiometric reduction eliminated complications to the kinetics from side reactions with excess dithionite. Reduction was followed by the loss of yellow color and fluorescence. Reduction was confirmed spectrophotometrically. Reduction could also be achieved photochemically using a solution of enzyme buffer with EDTA (9 mM) and a catalytic amount of 5-deazaflavin (1 μM) (Massey & Hemmerich, 1978).

Reoxidation of Reduced S229A Mutant Enzyme. S229A mutant enzyme was first made anaerobic in an anaerobic cuvette and subsequently reduced slightly less than stoichiometrically with a 10 mM solution of dithionite. Reoxidation was initiated by addition of either EP-UDP-GlcNAc (100 μM) or $NADP^+$ (50 μM) from the side arms. The reoxidation was followed in a Hewlett-Packard diode array spectrophotometer over the course of 2 days.

Rate of Isomerization of (E)-EB-UDP-GlcNAc to (Z)-EB-UDP-GlcNAc for S229A. The isomerization of *(E)*-EB-UDP-GlcNAc to *(Z)*-EB-UDP-GlcNAc was measured using an NMR assay under aerobic conditions at 25 °C. Briefly, two reaction mixtures each containing 3 mM *(E)*-EB-UDP-GlcNAc and 3.4 mM NADPH in 3 mL of Tris-HCl, pH 8.0, and 20 mM KCl were prepared in H_2O. Wild-type enzyme (2.3 μL of 20 mg/mL, 1.2 nmol) and S229A mutant enzyme (300 μL of 6.5 mg/mL, 51.5 nmol) were added to the reaction mixtures respectively. Samples (500 μL) were spun through spin columns to remove enzyme at each time point in order to quench the reaction. D_2O (500 μL) was added to the samples before analysis. Ratios of *(Z)*-EB-

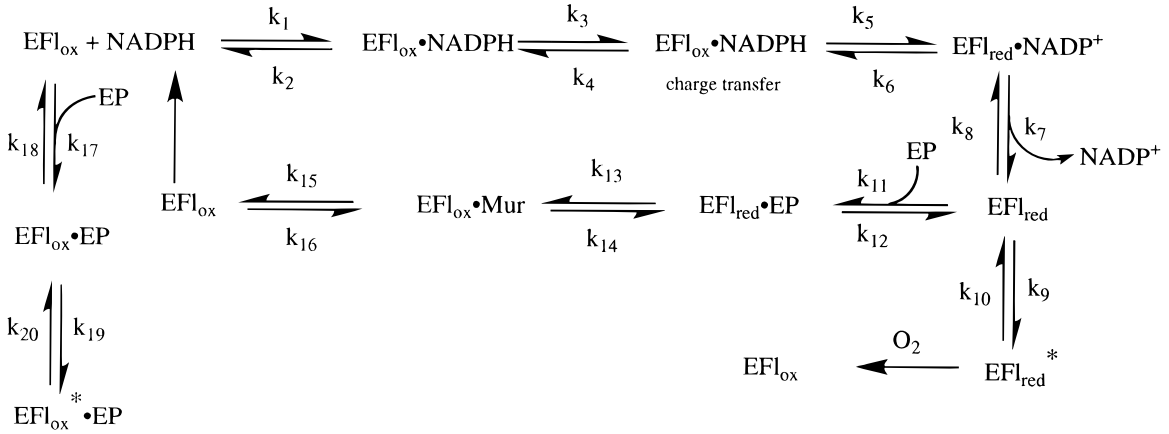

FIGURE 4: Proposed kinetic mechanism for the reductive and oxidative reactions of MurB. The scheme also includes the formation of an abortive complex of EP-UDP-GlcNAc with oxidized enzyme.

UDP-GlcNAc and UDP-Me-MurNAc were determined by integration.

Kinetics of Binding and Determination of K_d. Rates of binding of EP-UDP-GlcNAc, *(E)*-EB-UDP-GlcNAc, and $NADP^+$ to oxidized enzyme were monitored in the stopped-flow spectrophotometer at 513 nm, where the greatest increase in absorbance upon binding occurred, as determined from a difference spectrum between the bound and unbound spectra. Static titrations with each ligand were also carried out by monitoring the spectral shift of the flavin absorbance upon binding by measuring the change in absorbance of two wavelengths on either side of the 463-nm peak.

RESULTS

Production, Purification, and Steady-State Catalytic Parameters of S229A. Wild-type MurB was overproduced and purified according to methods described previously (Benson et al., 1993, 1994). The S229A mutant was overproduced and purified after ammonium sulfate precipitation in a similar manner by G-25 size exclusion, fast-flow Q-Sepharose, butyl-Sepharose, and 2′,5′-ADP-Sepharose without difficulty. The purity of S229A mutant enzyme was greater than 95% by SDS−PAGE analysis, which is comparable to wild-type purity. The overall yield of the S229A mutant was around 16 mg of pure enzyme from 1 L of cells, representing a 2-fold decrease in the amount of protein obtained from overproduction of the wild-type protein.

Steady-state kinetic analysis of the S229A MurB mutant using the aerobic NADPH spectrophotometric assay (Benson et al., 1993) showed the mutant to be catalytically impaired in turnover, oxidizing NADPH at a rate 0.01% of wild type. As this rate was extremely slow and likely included some competing NADPH oxidase activity (O_2 reoxidation of E•$FADH_2$), anaerobic methods were employed to study this mutant.

Reduction of MurB by NADPH and 4S-^{2}H-NADPH. The reductive half-reaction (EFl_{ox}-NADPH → EFl_{red}-$NADP^+$) of MurB was monitored at selected wavelengths from 340 to 750 nm but chiefly at two wavelengths, 463 and 540 nm. The proposed kinetic model for wild-type MurB is shown in Figure 4. The initial decrease in absorbance at 463 nm (Figure 5) coincides temporally with the formation of a transient EFl_{ox}-NADPH charge transfer complex (Massey & Ghisla, 1974), detected as an increase in absorbance at 540 nm (corresponding to k_3). Formation of this charge transfer complex also leads to a rapid and significant quenching of the flavin fluorescence. This rate was unaffected by varying the concentration of NADPH. Upon formation of the charge transfer complex, a major decrease in absorbance follows corresponding to the actual reduction step to form EFl_{red}-$NADP^+$ (corresponding to k_5). The reduction of the flavin cofactor was also observed as further quenching of the fluorescence.

A third rate constant, corresponding to k_7, was apparent from both the absorbance and fluorescence data, which was indicative of release of $NADP^+$ to form free E_{red}. Observation of this step is critical to our understanding of the kinetic mechanism of MurB for it is in fact the rate-limiting step during reduction by protio-NADPH. A fourth, slower phase (k_9) was observed during absorbance and fluorescence stopped-flow comprising less than 5% of the total absorbance change at 463 nm on the order of 0.4−0.6 s^{-1}. This final phase most likely reflects an isomerization of the reduced form of the enzyme EFl_{red} to EFl_{red}*, which is responsible for the reaction with molecular oxygen. Rate constants obtained from fitting of the absorbance and fluorescence traces for these kinetic steps are given in Table 1.

The deuterium isotope effect for transfer of deuteride from 4*S*-^{2}H-NADPH compared to hydride transfer from NADPH during catalytic turnover experiments was 3.2 (see below). This ^DV for the overall reaction is in contrast to the intrinstic ^DV of ∼5 for the reductive half-reaction. The fractional transmission of the isotope effect results from a shift of the rate-limiting step from the release of $NADP^+$ from E_{red} (k_7) in the case of protio-NADPH to the rate-limiting step being the transfer of deuteride (k_5) in the case of 4*S*-^{2}H-NADPH.

Comparison of the wild-type and S229A mutant enzymes revealed a decrease in the rate of the reduction of the bound FAD by a factor of 9 (Table 1). The rate of formation of the NADPH•FAD charge transfer complex remained on the order of 700 s^{-1} and the K_d values for NADPH and 4*S*-^{2}H-NADPH were on the order of 1 μM. The magnitude of the deuterium isotope effect with 4*S*-^{2}H-NADPH was reduced in the S229A mutant. Comparison of the redox potential of the FAD bound to wild-type and S229A mutant MurB gave values of −234 and −238 mV (pH 7.0, 25 °C) for the $E^{\circ\prime}$ values, indicating that the mutation had no substantial effect on the thermodynamics of reduction.

Steady-State Kinetics of NADPH-EP-UDP-GlcNAc Reductase Activity. The steady-state kinetics were measured by

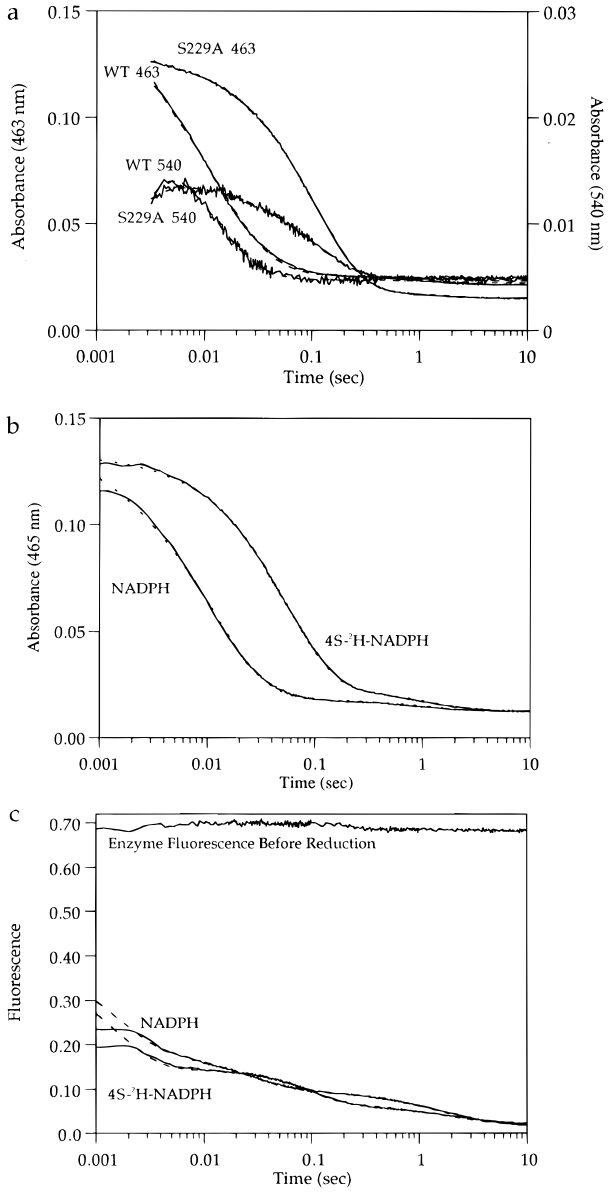

FIGURE 5: Rapid reaction kinetic data (solid lines) from the reductive half-reaction for MurB with curve fits (dashed lines) to constants in Table 1. (a) Absorbance data at 463 and 540 nm for the reduction of wild-type (11.0 μM) and S229A mutant (11.0 μM) enzyme (NADPH concentration 30 μM). (b) Absorbance data at 465 nm for the reduction of wild-type enzyme (12.0 μM) with protio-NADPH (43 μM) and 4*S*-^{2}H-NADPH (35 μM). (c) Fluorescence data for the reduction of wild-type enzyme (2.9 μM) with protio-NADPH (9.5 μM) and 4*S*-^{2}H-NADPH (10.5 μM). The top trace shows the fluorescence of the oxidized enzyme mixed with buffer instead of NADPH. The excitation wavelength for these experiments was 465 nm and the fluorescence emission was detected with a filter which cuts off light below 485 nm. In all panels the concentrations given are those after mixing in the stopped-flow apparatus.

making use of the rapid mixing capacity in the stopped-flow spectrophotometer under anaerobic conditions in order to exclude any complications from a competing oxygen reductase activity. Typically, enzyme at a final concentration of 0.6 μM was reacted with various combinations of concentrations of NADPH and EP-UDP-GlcNAc. The oxidation of NADPH was followed at 340 nm. The resulting data were analyzed in two ways. First, the initial rate of the reaction was determined. Second, the complete reaction trace was analyzed by determining tangents to the curve at regular time

Table 1: Rate Constants for Kinetic Mechanism[a]

	wild type		S229A	
	NADPH	4*S*-^{2}H-NADPH	NADPH	4*S*-^{2}H-NAPDH
k_2/k_1	~1 μM	~1 μM	~1 μM	~1 μM
k_3	700 s^{-1}	700 s^{-1}	700 s^{-1}	700 s^{-1}
k_5	90 s^{-1}	17 s^{-1}	10 s^{-1}	5 s^{-1}
k_7	35 s^{-1}	35 s^{-1}	35 s^{-1}	35 s^{-1}
k_8	12 s^{-1}		5×10^{-6} s^{-1}	
k_9	0.6 s^{-1}	0.6 s^{-1}	0.6 s^{-1}	0.6 s^{-1}

	wild type		S229A
	EP-UDPGlcNAc	EEB-UDP-GlcNAc	EP
k_{12}/k_{11}	9 μM	16 μM	
k_{13}	66 s^{-1}	0.5 s^{-1}	8×10^{-6} s^{-1}
k_{18}/k_{17}	33 μM		
k_{19}	400 s^{-1}		
k_{20}	40 s^{-1}		

[a] See Figure 4 for mechanism. Reaction conditions were 0.05 M Tris buffer, pH 8.0, and 20 mM KCl at 25 °C.

intervals giving a succession of values representing the apparent turnover number at finite concentrations of NADPH. This analysis allows construction of Lineweaver−Burk plots as a function of the remaining NADPH concentration (Figure 6b,c) or remaining EP-UDP-GlcNAc concentration (Figure 6a). The results show marked inhibition by high concentrations of EP-UDP-GlcNAc in agreement with results of Dhalla et al. (1995). This inhibition is nicely explicable in terms of an abortive complex between oxidized enzyme and EP-UDP-GlcNAc as proposed by Dhalla et al. (1995) and is documented in a following section. This kinetic scheme predicts a competitive inhibition between EP-UDP-GlcNAc and NADPH consistent with the results shown in Figure 6. The intercept of such plots should therefore define the true k_{cat} value in the absence of the inhibitory effect. Lineweaver−Burk plots of e/v versus 1/EP-UDP-GlcNAc are expected to show marked inhibition when the concentration of EP-UDP-GlcNAc approaches that of its K_i value, as observed in Figure 6a. At low concentrations of EP-UDP-GlcNAc the double-reciprocal plots are expected to be linear, extrapolating at high concentrations of NADPH to values close to that of k_{cat}. The value of k_{cat} obtained is ~1400 min^{-1} (24 s^{-1}). A pronounced deuterium isotope effect was observed when 4*S*-^{2}H-NADPH is used instead of protio-NADPH, giving a k_{cat} of ~430 min^{-1} (7 s^{-1}).

Steady-State Kinetics of NADPH−O_2 Reductase Activity. Catalytic turnover of NADPH employing O_2 as the electron acceptor was also followed in the stopped-flow spectrophotometer, where enzyme was mixed with NADPH solutions equilibrated with various concentrations of O_2. In distinction to the results obtained with the natural substrate, the observed rates were essentially independent of both O_2 concentration and NADPH concentration with a limiting turnover number of 44 ± 3 min^{-1}. Surprisingly, the results were also independent of whether protio- or deutero-NADPH was used as substrate. The implications of these results will be considered further in the discussion.

Binding of EP-UDP-GlcNAc, (E)-EB-UDP-GlcNAc, and NADP to $MurB_{ox}$. During kinetic studies, it became apparent that the binding of the normal substrate EP-UDP-GlcNAc, the alternate enolbutyryl substrate *(E)*-EB-UDP-GlcNAc, and the product $NADP^+$ to the oxidized form of the enzyme are kinetically significant factors in the catalytic mechanism of MurB. The binding of all three compounds to the oxidized

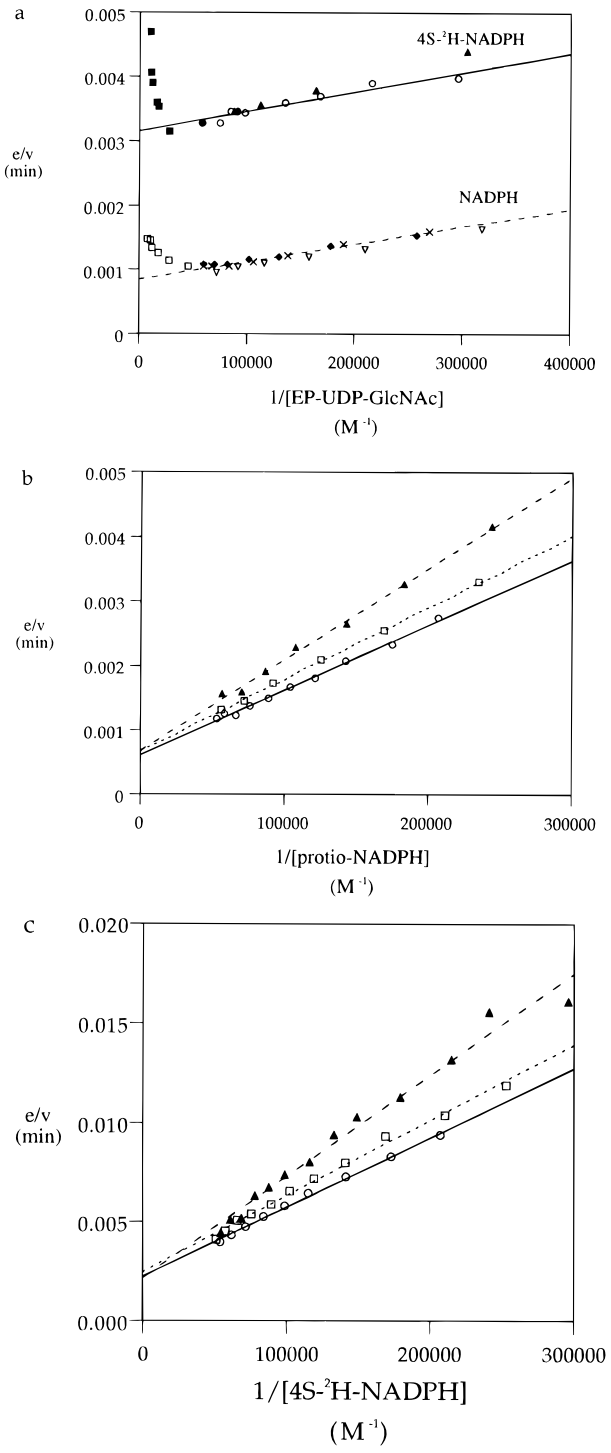

FIGURE 6: Steady-state analysis of the NADPH-EP-UDP-GlcNAc reductase activity. (a) Squares shown are values of initial rates with EP-UDP-GlcNAc in excess of NADPH (21.3 μM). Other points were obtained by analysis of the complete reaction curves as described in the text. (b, c) Data obtained from the analysis of the complete reaction curves for 110 μM EP (top line), 73 μM EP (middle line), and 55 μM EP (bottom line). In each case the starting concentration of NADPH was 41.3 μM for protio-NADPH and 20.8 μM for 4*S*-^{2}H-NADPH. The reaction was followed until all the NADPH was consumed.

form of the enzyme was monitored both statically in equilibrium titrations and kinetically by stopped-flow spectrophotometry utilizing the corresponding red shift of the bound FAD observed upon ligand binding. This shift lead to a change in the absorbance maximum from 463 to 472 nm. Inconsistencies of K_d values obtained from static

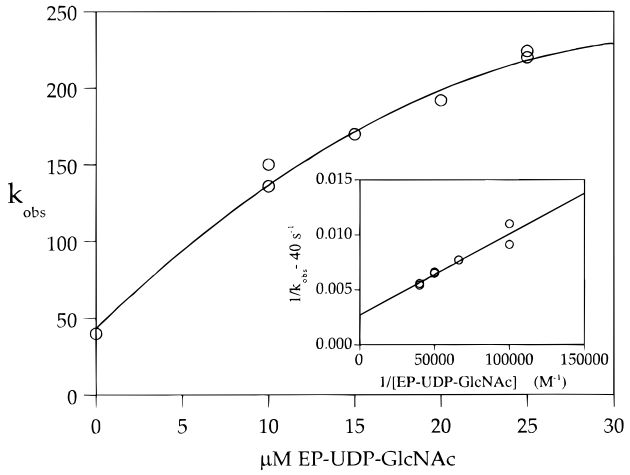

FIGURE 7: Kinetics of binding of EP-UDP-GlcNAc to EFl_{ox} to form the abortive complex. Enzyme (concentration = 4.2 μM) was reacted in a stopped-flow spectrophotometer with the concentrations of EP-UDP-GlcNAc as shown. The increase in absorbance at 530 nm was monitored to yield the values of k_{obs} as shown. The values of k_{obs} at the intercept was obtained in a separate experiment as described in the text. The inset shows a linear transform of the data as described in Strickland et al. (1975).

Table 2: Dissociation Constants for Binding of Ligands to Oxidized MurB[a]

ligand	enzyme	K_d (μM)
$NADP^+$	wild type	2.4
	S229A	2.5
EP-UDP-GlcNAc	wild type	4.1
	S229A	7.3
EEB-UDP-GlcNAc	wild type	5.9
	S229A	5.3

[a] K_d values were determined by calculating $K_d = [L_f][E_f]/[EL]$ from static spectrophotometric titrations using a Hewlett-Packard diode array spectrophotometer.

equilibrium titrations of the enzyme with ligands compared to those obtained from kinetic data assuming a single-step binding indicated that, in fact, the binding of these ligands involves a two-step equilibrium. Representative data for the binding of EP-UDP-GlcNAc to EFl_{ox} are shown in Figure 7. A limiting value of k_{off} for the binding of EP-UDP-GlcNAc was obtained from experiments in which the oxidized enzyme was equilibrated with EP-UDP-GlcNAc (60 μM) and then reacted anaerobically with NADPH in the stopped-flow spectrophotometer. The approach to steady state was defined by a rate constant, k_{20}, of 40 $\pm$ 1 s^{-1} independent of the concentration of NADPH (50−150 μM). Under the same conditions, when uncomplexed enzyme was reacted with a mixture of EP-UDP-GlcNAc and NADPH, the approach to steady state was defined by a rate constant of approximately 160 s^{-1}. The observed rate constant of binding of EP-UDP-GlcNAc thus shows a hyperbolic relationship (Figure 7) indicating a two-step equilibrium binding process. Analysis of the data by the method of Strickland et al. (1975) shown in the inset yields the values shown in Table 1 for the rate constants defined in Figure 4. The K_d overall for this two-step binding process $k_{18}k_{20}/k_{17}(k_{19} + k_{20})$ is 3.1 μM, in good agreement with the value of 4.1 μM obtained by static equilibrium titration. The binding of the other ligands listed in Table 2 was also measured in the stopped-flow spectrophotometer and found to be equally rapid. As in the case of EP-UDP-GlcNAc, the apparent

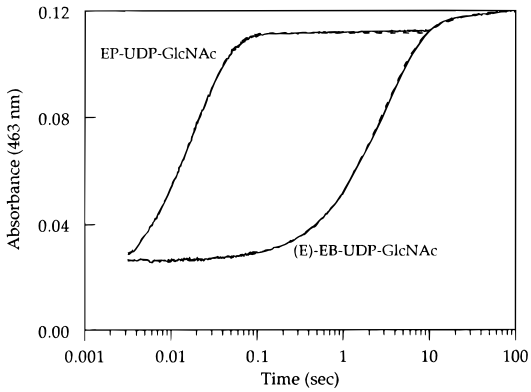

FIGURE 8: Rapid reaction kinetic data (solid lines) for the oxidative half-reaction with curve fits (dashed lines) to constants in Table 1 for wild-type MurB (10.2 μM) with EP-UDP-GlcNAc (40 μM) and *(E)*-EB-UDP-GlcNAc (40 μM) monitored at 463 nm. In all panels the concentrations given are those after mixing in the stopped-flow apparatus.

discrepancy between the values of K_d calculated from the apparent ratio of k_{off}/k_{on} compared to those obtained by static equilibrium titrations indicates similar two-step binding processes. However, in these cases the full kinetic analyses have not been carried out. No dramatic differences were observed between the binding of ligands to wild-type and S229A mutant enzyme, suggesting that integrity of molecular recognition is not affected in the S229A mutant.

Reoxidation of Reduced MurB. The reoxidation of wild-type enzyme (E•FADH$_2$ → E•FAD) by the enolpyruvyl and the *(E)*-enolbutyryl substrates, EP-UDP-GlcNAc and *(E)*-EB-UDP-GlcNAc, was clearly monophasic (Figure 8) with rate constants of 66 s^{-1} and 0.5 s^{-1}, respectively (Table 1). The 132-fold decrease in the rate of reoxidation of the reduced flavin by *(E)*-EB-UDP-GlcNAc compared to EP-UDP-GlcNAc is consistent with the approximately 100-fold decrease in the rate of formation of the reduced product UDP-Me-MurNAc compared to UDP-MurNAc (Lees et al., 1996). The corresponding K_d values for EP-UDP-GlcNAc and *(E)*-EB-UDP-GlcNAc substrates in this half-reaction were 9 μM and 16 μM, respectively.

The S229A mutant enzyme revealed a striking reduction on the order of 10^6-10^7-fold in the rate of FADH$_2$ reoxidation with both EP-UDP-GlcNAc and NADP$^+$ as substrates. In constrast to wild-type enzyme, where reoxidation is complete in the millisecond time range, the S229A mutant requires hours to days (Table 1). The dramatic 10^7-fold decrease in EFl$_{red}$ reoxidation rate with EP-UDP-GlcNAc revealed that S229A mutant has a specific defect in the reoxidation of FADH$_2$ and hence the reduction of the enol pyruvyl moiety. Reoxidation of the FADH$_2$ species by NADP$^+$ in the S229A mutant enzyme was also decreased by approximately 7 orders of magnitude when compared with wild-type enzyme, suggesting that Ser 229 is somehow also involved with reoxidation by NADP$^+$. It is unclear at this time how Ser 229 is specifically involved in NADP$^+$ reoxidation, as more information about the location of the nicotinamide binding site is needed to adequately interpret this result. During the course of this slow redox reaction, no charge transfer bands were detected between 500 and 800 nm to indicate a carbanion-FAD charge transfer complex. Surprisingly, the reoxidation rate was increased at least 20-fold when NADP$^+$ and EP-UDP-GlcNAc were both present during reoxidation.

Table 3: NMR Rate Constants in H_2O for Catalysis Using the Alternate Substrate EEB-UDP-GlcNAc

enzyme	reduction rate (s^{-1})	isomerization rate (s^{-1})
wild type	0.185	0.043
S229A	3.4×10^{-4}	3.1×10^{-3}

Isomerization of (E)-EB-UDP-GlcNAc to (Z)-EB-UDP-GlcNAc. The product-determining solvent isotope effect on the isomerization of *(E)*-EB-UDP-GlcNAc to *(Z)*-EB-UDP-GlcNAc described in Lees et al. (1996) suggested one additional means to investigate the effect of the S229A mutant. As catalysis in D_2O increased the proportion of isomerized product for wild-type enzyme, the S229A mutation should have an analogous effect. The ability of the S229A MurB to isomerize the double-bond geometry in *(E)*-EB-UDP-GlcNAc was tested in an NMR assay. The S229A mutant catalyzed the conversion of *(E)*-EB-UDP-GlcNAc to *(Z)*-EB-UDP-GlcNAc at an overall rate which was 7.2% of wild type (Table 3). The product ratio [UDP-MeMurNAc: *(Z)*-EB-UDP-GlcNAc] for wild type was 4.3:1 in favor of the reduced product and for S229A was 1:9.2 in favor of the isomerized product.

The 14-fold reduction in isomerization activity with the mutant enzyme corresponds approximately to the decrease in rate observed for the reductive half-reaction of the S229A mutant and may reflect the kinetics of formation of the FADH$_2$ species. In contrast, the rate of formation of reduced product is severely diminished (over 500-fold) from the wild-type rate of formation of UDP-Me-MurNAc (Table 3). Yet, this rate of product formation is still too fast to be consistent with the 8×10^{-6} s^{-1} rate of reoxidation of FADH$_2$ observed in the anaerobic cuvette assay. Hence, most of the reductive flux observed in the NMR assay with S229A probably represents the presence of contaminating wild-type enzyme in the S229A mutant sample.

This result is not surprising because the S229A mutant enzyme was necessarily overproduced in a wild-type *Escherichia coli* strain due to the essential nature of the gene product. The level of wild-type contamination can be accounted for by the following argument. The rate of directly observed reoxidation of the S229A FADH$_2$ by the natural substrate EP-UDP-GlcNAc is on the order of 10^{-6} s^{-1} (Table 1). Since this rate and all the rate constants for S229A were determined by following flavin spectral changes rather than NADPH oxidation or UDP-MurNAc formation, the rates for the primary population, the S229A mutant enzyme, could be determined despite the presence of a small percentage of wild-type enzyme. Since in wild-type enzyme the rate of reoxidation by *(E)*-EB-UDP-GlcNAc is roughly 100-fold down from EP-UDP-GlcNAc-mediated reoxidation, one would predict the rate of reoxidation by *(E)*-EB-UDP-GlcNAc to be on the order of 10^{-8} s^{-1}, 4 orders of magnitude below the rate (3.4×10^{-4} s^{-1}) observed in the NMR assay. A 1.8% contamination of S229A MurB by wild-type MurB would be enough to account for the production of UDP-Me-MurNAc at the rate observed in the NMR experiment. This level of contamination would also mean that 5% of the *(Z)*-EB-UDP-GlcNAc formed during the assay resulted from the wild-type enzyme [not a significant detractor in determining the rate of formation of *(Z)*-EB-UDP-GlcNAc by S229A MurB]. If there is indeed a contamination of 1.8% wild-type MurB in the S229A sample and the k_{cat} for UDP-Me-

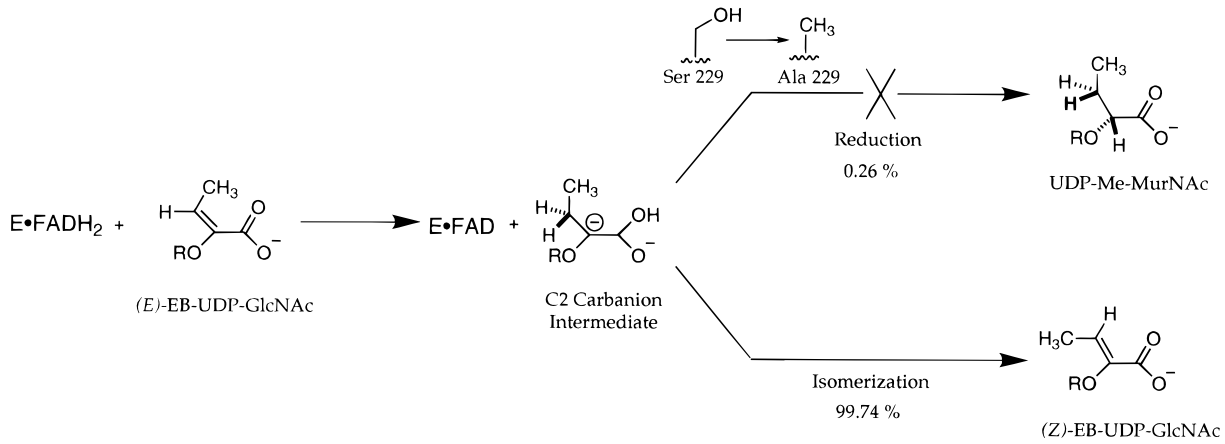

FIGURE 9: Schematic of the partitioning of *(E)*-EB-UDP-GlcNAc between reduction and isomerization in the S229A MurB mutant. The reductive flux is effectively blocked by this single mutation (see text for discussion).

MurNAc formation by S229A MurB is $\approx 10^{-6}$ s^{-1}, then $k_{isomerization}/k_{reduction} \approx 10^3$ for S229A MurB compared to a ratio of 0.2 for wild-type MurB. The partitioning ratio is dramatically altered in favor of isomerization in S229A due to the selective slowing of the rate of protonation of the enol intermediate (Figure 9).

DISCUSSION

Kinetic Mechanism. The results of the rapid reaction studies of the reductive and oxidative half-reactions of MurB combined with steady-state analysis are summarized in Figure 4 and Table 1. The ability of the oxidized enzyme to form a complex with EP-UDP-GlcNAc results in severe inhibition at high concentrations and complicates the steady-state kinetic analysis. The formation of the abortive complex was shown to involve a two-step equilibrium binding, the first step being a rapid equilibrium (k_{18}/k_{17}) of 33 μM followed by a rapid isomerization step ($k_{19} = 400$ s^{-1}) and a reverse step ($k_{20} = 40$ s^{-1}). These rate constants are comparable to those involved in the binding of NADPH to the oxidized enzyme (k_1, k_2, k_3, and k_4) and so could account for the observed inhibition. It should be noted that the inhibition constant for EP-UDP-GlcNAc observed in steady-state kinetics measurements is $\sim$200 μM, similar to that observed by Dhalla et al. (1995) and much greater than the K_d value of 3−4 μM for binding of EP-UDP-GlcNAc to oxidized enzyme. This apparent discrepancy can be accounted for if the rate constants associated with binding of NADPH are in fact greater than those associated with the binding of EP-UDP-GlcNAc. This phenomenon is consistent with the rapid quenching of the enzyme flavin fluorescence observed in stopped-flow experiments. Studies on the separate reductive half-reaction in the absence of EP-UDP-GlcNAc reveal a very rapid equilibrium binding of NADPH, follwed by a very rapid formation of a charge transfer complex between oxidized enzyme and NADPH. This is particularly evident in the fluorescence data where large quenching of the fluorescence is associated with the rapid binding. The charge transfer complex (particularly evident in the absorbance studies in the 500−600-nm range) precedes the reduction of the flavin (k_5) and dissociation of product NADP$^+$ (k_7) and is followed further by an isomerization reaction of the free reduced enzyme (k_9 and k_{10}). Estimates of the values of the individual rate constants obtained from curve fitting of the absorbance (Figure 5a,b) and the fluorescence (Figure 5c) data are shown in Table 1. The k_{cat} value for protio-NADPH and EP-UDP-GlcNAc of 24 s^{-1} is within experimental error, consistent with the limiting rates of formation of free reduced enzyme and reoxidation by EP-UDP-GlcNAc (Table 4). Similarly, the K_m values for NADPH and EP-UDP-GlcNAc are consistent with the proposed mechanism (Table 4). It should be emphasized, however, that while a ping-pong mechanism with abortive complex binding of EP-UDP-GlcNAc to oxidized enzyme appears to be consistent with all the data, the insensitivity of catalytic velocity to variation of NADPH concentration and the inhibition by EP-UDP-GlcNAc make it difficult to be certain that this is indeed the kinetic mechanism. However, the observation of a NADPH concentration-independent rate constant of 40 s^{-1} when enzyme was prequilibrated with EP-UDP-GlcNAc, equatable with a limiting rate of dissociation of EP-UDP-GlcNAc, implies that NADPH can react only when EP is not bound, consistent with a ping-pong kinetic mechanism. Structural analysis from the substrate-free form of the enzyme (Benson et al., 1996) which shows a single, prominent channel leading into the active site, which is in fact the EP-UDP-GlcNAc binding site, also is consistent with a ping-pong kinetic mechanism.

Table 4: Comparison of Steady-State Kinetics Parameters with Those Derived from Rapid Reaction Studies[a]

	protio-NADPH	4*S*-^{2}H-NADPH
k_{cat}	24 s^{-1}	7 s^{-1}
K_m^{NADPH}	$<10^{-6}$ M	$<10^{-6}$ M
$K_m^{EPUDPGlcNAc}$	$\sim 3.5 \times 10^{-6}$ M	$\sim 1.5 \times 10^{-6}$ M
Predicted Kinetics Parameters from Measured Rate Constants		
$k_{cat} = k_{red}k_{ox}/(k_{red} + k_{ox})$	$= (25.2\text{ s}^{-1})(66\text{ s}^{-1})/(91.2\text{ s}^{-1})$ $= 18.2$ s^{-1}	$= (11.4\text{ s}^{-1})(66\text{ s}^{-1})/(77.4\text{ s}^{-1})$ $= 9.7$ s^{-1}
$K_m^{NADPH} \approx (k_2/k_1)(k_{cat}/k_{red})$	$<10^{-7}$ M	$<10^{-7}$ M
$K_m^{EP} \approx (k_{12}/k_{11})(k_{cat}/k_{ox})$	$= 2.5 \times 10^{-6}$ M	$= 1.3 \times 10^{-6}$ M

[a] k_{red} was obtained from the relationship $1/k_{red} = 1/k_5 + 1/k_7$ and $k_{ox} = k_{13}$.

The surprising result from the kinetic analysis is the lack of an observed isotope effect in the NADPH−oxygen reductase activity. The reaction of reduced enzyme with oxygen was found to occur with a second-order rate constant of 1.3×10^4 M^{-1} s^{-1} (data not shown). The observed k_{cat} of 40 min^{-1} (0.6 s^{-1}) coincides with the rate of the isomerization reaction observed in the reductive half-reaction studies. This step (Figure 4, k_9) is thus insensitive to the

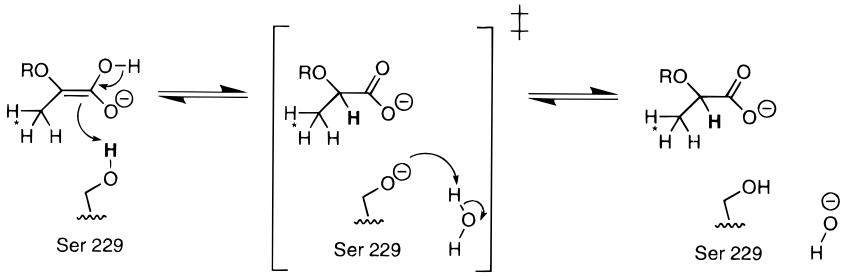

FIGURE 10: Protonation of the enol/carbanion intermediate by Ser 229. H* at C3 originates on NADPH. The alkoxide anion transition state is proposed to be reprotonated by a specific water found in the active site [see accompanying paper (Benson et al., 1997)].

deuterium isotope effect on reduction (k_5) and nicely accounts for the observed results. The results clearly show that the reduced enzyme can exist in two forms, presumably conformationally different, one of which is capable of reacting with the natural acceptor EP-UDP-GlcNAc, while only the slowly produced form is able to react with molecular oxygen.

S229A MurB Kinetics. Analysis of the S229A mutant in the routine steady-state assay which measures NADPH oxidation indicated that the mutant k_{cat} was virtually immeasurable. In such cases, it is useful to assess partial reactions to see if the enzyme suffers from any general defect such as misfolding and attempt to isolate the effect of the mutation to a specific half-reaction. In flavoproteins, one has the distinct advantage of monitoring rates of reduction and reoxidation of the bound flavin cofactor to assess the impact of mutations on a specific partial reaction.

By this criterion, S229A is only marginally impaired in the rate of hydride transfer from NADPH to FAD, indicating that the nicotinamide portion of the active site and catalytic apparatus are still reasonably intact. The minimal difference in the reduction potentials of wild-type and S229A mutant MurB indicates that the S229A mutation did not affect the thermodynamics of the FAD redox process. A decrease in the reduction rate by a factor of 9 in S229A MurB suggests that Ser 229 plays some role in the reduction of FAD, perhaps to provide a stabilizing hydrogen bond in the hydride transfer step from NADPH to FAD. Such an effect would be consistent with observations from the substrate-free MurB X-ray crystal structure (Benson et al., 1996), which reveals a channel leading into the active site and would place the nicotinamide on the *si* face of the isoalloxazine ring in the vicinity of Ser 229.

In contrast, the effect of the reoxidative half-reaction, the rate of hydride transfer from $FADH_2$ to EP-UDP-GlcNAc, is dramatic. The approximately 10^7-fold rate decrease in reoxidation of the $FADH_2$ allows us to focus on this aspect of the chemistry and the associated active-site architecture for specifically impaired electron transfer to the olefin cosubstrate. Such a large rate decrease for reoxidation strongly suggests Ser 229 plays a major role in reprotonation of the C2 carbanion.

One additional powerful indication that S229A is selectively impaired in its ability to reprotonate the nascent product C2 carbanion is the dramatic change in partition experienced by *(E)*-EB-UDP-GlcNAc between reduction to UDP-Me-MurNAc and isomerization to the *Z* double-bond geometric isomer (Figure 9). The upper arm of Figure 9—partitioning to the reduced product UDP-Me-MurNAc—requires C2 protonation, presumably by Ser 229. This partitioning has been decreased such that the flux through the upper arm is now only 0.26% in S229A, compared to 81% in wild type. As C2 protonation is selectively slowed, the C2 carbanion can rotate around the C2−C3 single bond followed by the transfer of hydride from C3 back to N5 of FAD and release of the *Z* double-bond geometric isomer. This lower arm accounts for 99.74% of the flux in the S229A mutant.

Reduction of Olefins by Flavoproteins. From the structure of other flavoproteins that reduce carbon−carbon double bonds, the best precedents for active-site proton donors to C2 during olefin reduction are provided by the acyl-CoA desaturases. The active site of medium-chain acyl-CoA dehydrogenase from pig liver mitochondria reveals an octanoyl-CoA molecule sandwiched between the FAD cofactor and Glu 376 (Kim et al., 1993). The carboxylate oxygens are 4.2−4.6 Å away from the C2 position. A similar active-site positioning of Glu 376 is seen in the butyryl-CoA dehydrogenase from *Megasphaera elsdenii* (Djordjevic et al., 1995). The structural prediction for Glu 376 as the proton donor/abstractor has been confirmed by mutagenesis of Glu 376 to Gln in human medium-chain acyl-CoA dehydrogenase (Bross et al., 1990) and *M. elsdenii* butyryl-CoA dehydrogenase (Becker et al., 1993). The mutant activities are less than 0.02% and 0.03% of wild type, respectively. Therefore, it is reasonable that Glu 376 is a structurally, kinetically, and thermodynamically viable proton donor.

Ser 229, the proposed proton donor in MurB, is located in an analogous position as the acyl-CoA dehydrogenase Glu 376. Precedent exists for deprotonation of serine residues in catalytic transition states for serine proteases, although in these cases serine goes on to function as a nucleophile (alkoxide) and not as a proton donor. During MurB catalysis, we propose that Ser 229 functions not in a nucleophilic catalysis but rather in acid−base catalysis (with alkoxide reprotonation by a specifically positioned active-site water molecule) [Figure 10 and see accompanying paper (Benson et al., 1997)]. *A priori*, serine is less likely to function as a proton transfer agent than glutamic acid because of its high pK_a value. Yet, the pK_a of a proton α to a carboxylate (the proton at C2 of the lactyl ether moiety) is around 22 (Gerlt & Gassman, 1992), making the ΔpK_a between serine and C2 of the product favorable for proton transfer. Three kinds of evidence summarized below, precedent, rate, and location, point to the function of Ser 229 as the proton donor which quenches the carbanion intermediate.

Precedent for Serine as a Proton Donor. The role of serine as a proton donor has been proposed in one other enzymatic system. The serine hydroxyl moiety has been postulated as a proton donor in the photosynthetic reaction centers of both *Rhodopseudomonas viridis* (Leibl et al., 1993) and *Rhodobacter sphaeroides* (Paddock et al., 1990). This

transmembrane protein complex in photosynthetic bacteria utilizes light energy for electron transfer and proton uptake (Feher et al., 1989). During the electron cascade, electrons are passed through a series of protein-bound cofactors. One transformation involves the formation of dihydroquinone from quinone. The structures of the active sites of *Rps. viridis* (Deisenhofer et al., 1995) and *Rb. sphaeroides* (Allen et al., 1988) show Ser 223 of the L domain within hydrogen-bonding distance (2.7 Å) to one of the carbonyl oxygens of the quinone. Serine to alanine mutants in the photoreaction center of both species lead to a 350−600-fold decrease in activity (Leibl et al., 1993; Paddock et al., 1990).

Kinetic Evidence. The impaired turnover in the S229A mutant strongly suggests that the serine hydroxyl is required for reduction of the enolpyruvyl moiety. The approximately 10^7-fold decrease in rate seen for the reoxidation of the reduced flavin isolates the effect of the mutation to the second half-reaction, namely, reoxidation with either EP-UDP-GlcNAc or $NADP^+$. The rate effects could be the result of an alteration of the substrate binding site, yet static titration experiments monitoring the binding of EP-UDP-GlcNAc, *(E)*-EB-UDP-GlcNAc, and $NADP^+$ demonstrated that the K_d values for these substrates were not significantly changed in the S229A mutant enzyme.

Location and Orientation. The position of Ser 229 in the active site of the EP-UDP-GlcNAc-MurB X-ray crystal structure (Benson, et al., 1995) first suggested that it may play a role as a general acid catalyst in the second half-reaction. Analysis of the active site showed Ser 229 only 3.2 Å away from C2 in a suitable location and orientation for stereospecific proton transfer. The active site of the EP-UDP-GlcNAc complex shows no other residue with the distance or orientation required for proton transfer [see accompanying paper (Benson et al., 1997)]. One water which is 4.3 Å away from C2 is too far away to be involved in direct protonation, but we note that this water (H_2O 500) and Ser 229 may function as a couple [Figure 10; see accompanying paper (Benson et al., 1997)].

The approximately 10^7-fold decrease in reduction of the olefin is truly dramatic given that the X-ray structure of the substrate−wild-type MurB complex shows a water molecule situated within 4.3 Å. It is possible that the enormous decrease in the reoxidation half-reaction of the EFl_{red} in S229A is due to a combination of effects that include absence of a specific proton donor hydroxyl group, altered hydrophilicity balance in the active site of S229A, and displacement or a different orientation of the active-site water molecule that sum to an increased barrier height of an additional 9.8 kcal/mol. Indeed, the X-ray crystal structure of S229A in complex with EP-UDP-GlcNAc described in the accompanying paper (Benson et al., 1997) indicates that structure of the active site remains essentially intact in the S299A mutant. Loss of the serine hydroxyl also leads to the absence of a single water molecule in the active site which was formerly hydrogen-bonded to the serine side chain. Therefore, the dramatic decrease in reoxidation of EFl_{ox} in the S229A mutant is a direct result of the absence of the serine hydroxyl and an associated well-defined water molecule and the disrupted hydrogen-bonding network within the active site.

ACKNOWLEDGMENT

We thank Dr. Watson J. Lees for his expert assistance in collecting NMR data for the *(E)*-EB-UDP-GlcNAc isomerization/reduction assay. We also thank members of the Walsh group for critical reading of the manuscript.

REFERENCES

Allen, J. P., Feher, G., Yeates, T. O., Komiya, H., & Rees, D. C. (1988) *Proc. Natl. Acad. Sci. U.S.A. 85*, 8487−8491.

Beaty, N. B., & Ballou, D. P. (1981) *J. Biol. Chem. 256*, 4611−4618.

Becker, D. F., Fuchs, J. A., Banfield, D. K., Funk, W. D., MacGillivray, R. T. A., & Stankovich, M. T. (1993) *Biochemistry 32*, 10736−10742.

Benson, T. E., Marquardt, J. L., Marquardt, A. C., Etzkorn, F. A., & Walsh, C. T. (1993) *Biochemistry 32*, 2024−2030.

Benson, T. E., Walsh, C. T., & Hogle, J. M. (1994) *Protein Sci. 3*, 1125−1127.

Benson, T. E., Filman, D. J., Walsh, C. T., & Hogle, J. M. (1995) *Nature Struct. Biol. 2*, 644−653.

Benson, T. E., Walsh, C. T., & Hogle, J. M. (1996) *Structure 4*, 47−54.

Benson, T. E., Walsh, C. T., & Hogle, J. M. (1997) *Biochemistry 36*, 806−811.

Bevington (1969) *Data Reduction and Error Analysis for the Physical Sciences*, McGraw Hill, Inc., New York.

Brissette, P., Ballou, D. P., & Massey, V. (1989) *Anal. Biochem. 181*, 234−238.

Bross, P., Engst, S., Strauss, A. W., Kelly, D. P., Rasched, I., & Ghisla, S. (1990) *J. Biol. Chem. 265*, 7116−7119.

Bugg, T. D. H., & Walsh, C. T. (1993) *Nat. Prod. Rep.* 199−215.

Dhalla, A. M., Yanchunas, J., Ho, H. T., Falk, P. J., Villafranca, J. J., & Robertson, J. G. (1995) *Biochemistry 34*, 5390−5402.

Deisenhofer, J., Epp, O., Sinning, I., & Michel, H. (1995) *J. Mol. Biol. 246*, 429−457.

Djordjevic, S., Pace, C. P., Stankovich, M. T., & Kim, J.-J. P. (1995) *Biochemistry 34*, 2163−2171.

Feher, G., Allen, J. P., Okamura, M. Y., & Rees, D. C. (1989) *Nature 339*, 111−116.

Gerlt, J. A., & Gassman, P. G. (1992) *J. Am. Chem. Soc. 114*, 5928−5934.

Gerlt, J. A., & Gassman, P. G. (1993) *Biochemistry 32*, 11943−11952.

Kim, J.-J. P., Wang, M., & Pashke, R. (1993) *Proc. Natl. Acad. Sci. U.S.A. 90*, 7523−7527.

Lees, W. J., & Walsh, C. T. (1995) *J. Am. Chem. Soc. 117*, 7329−7337.

Lees, W. J., Benson, T. E., Hogle, J. M., & Walsh, C. T. (1996) *Biochemistry 35*, 1342−1351.

Leibl, W., Sinning, I., Ewald, G., Michel, H., & Breton, J. (1993) *Biochemistry 32*, 1958−1964.

Massey, V. (1990) in *Flavins and Flavoproteins* (Curti, B., Ronchi, & S., Zanetti, G., Eds.) pp 59−66, Walter de Gruyter & Co., Berlin.

Massey, V., & Ghisla, S. (1974) *Ann. N.Y. Acad. Sci. 227*, 446−465.

Massey, V., & Hemmerich, P. (1978) *Biochemistry 17*, 9−17.

Paddock, M. L., McPherson, P. H., Feher, G., & Okamura, M. Y. (1990) *Proc. Natl. Acad. Sci. U.S.A. 87*, 6803−6807.

Park, J. T. (1987) in *Escherichia coli and Salmonella typhimurium: Cellular and Molecular Biology* (Neidhardt, F. C., Ingraham, J. L., Low, K. B., Magasanik, B., Schaechter, M., & Umbarger, H. E., Eds.) pp 663−671, American Society for Microbiology, Washington, DC.

Strickland, S., Palmer, G., & Massey, V. (1975) *J. Biol. Chem. 250*, 4048−4052.

Walsh, C. T. (1979) *Enzymatic Reaction Mechanisms*, W. H. Freeman and Company, New York.

BI962220O